Smart Materials and Structures

A novel noncontact electromagnetic field-based sensor for the monitoring of resonant fatigue tests

To cite this article: Si-Byung Nam *et al* 2011 *Smart Mater. Struct.* **20** 035005

Smart Mater. Struct. 20 (2011) 035005 (13pp) doi:10.1088/0964-1726/20/3/035005

A novel noncontact electromagnetic field-based sensor for the monitoring of resonant fatigue tests

Si-Byung Nam[1], Gun Jin Yun[2,5], Joan Carletta[3], Dong-Han Kim[4] and Wieslaw Binienda[2]

[1] Department of Electrical Engineering, Kangwon National University, Samchuck, Korea
[2] Department of Civil Engineering, The University of Akron, Akron, OH 44325, USA
[3] Department of Electrical and Computer Engineering, The University of Akron, Akron, OH 44325, USA
[4] Department of Electrical Engineering, Kyung Hee University, Yongin, Korea

E-mail: sbnam@kangwon.ac.kr, gy3@uakron.edu, carlett@uakron.edu, donghani@khu.ac.kr and wieslaw@uakron.edu

Received 28 September 2010, in final form 11 December 2010
Published 8 February 2011
Online at stacks.iop.org/SMS/20/035005

Abstract

In this paper, a prototype of an electromagnetic field-based (EFB) vibration sensor that uses a novel sensing technique to monitor the resonant fatigue testing of a conductive and/or ferromagnetic target specimen is presented. The distance from the target to a coil within the sensor affects the impedance of the coil. The electronic circuitry for the sensor consists of a relaxation oscillator, an embedded microprocessor module and a high-speed digital-to-analog converter. The impedance of the coil determines the frequency of oscillation of the relaxation oscillator's output, so that vibration of the target causes changes in the oscillation frequency. A timer in the embedded microprocessor module is used to count the oscillations, producing a digital signal that indicates the coil-to-target distance. The digital signal is instantaneously converted to an analog signal to produce the sensor's output. The key technologies proposed include: (1) a novel timer counting method using the input capture functionality and timer of the embedded microprocessor module and (2) significant simplification of the analog electronic circuitry. The performance of the proposed sensor has been verified using AISI 1095 carbon steel and Al6061–T6 aluminum alloy specimens during resonant fatigue tests. The sensor shows a good linearity between displacement amplitudes and output voltages.

(Some figures in this article are in colour only in the electronic version)

1. Introduction

The use of noncontact sensors for vibration monitoring eliminates the difficulties associated with modifying a host structure to accommodate contact sensors. Examples of noncontact sensors include inductive sensors [1–3], capacitive sensors [4], laser scanning vibrometers [5], and image sensors [6], among others. Noncontact sensors are commonly not affected by hysteresis associated with damage to host structures. Among the types of noncontact sensors, inductive sensors are particularly appropriate for sensing the motion of conductive and ferrous materials. They are highly durable, with wear-free characteristics. They are also less affected by humidity and dirty environments than capacitive sensors. Inductive sensors have been well accepted as proximity sensors for industrial automation [7–10]. Fericean *et al* presented recent technological innovations in an inductive linear displacement sensor [7]. Passeaub *et al* used an electrodeposited flat coil with an on-chip CMOS readout circuit for an angular position sensor [8]. In 1997, Passeaub *et al* used a differential relaxation oscillator with a low-cost flat coil, and presented relationships between the oscillator's output signal frequency and the coil-to-target distance [9].

[5] Address for correspondence: 244 Sumner Street ASEC 209F, Akron, OH 44325, USA.

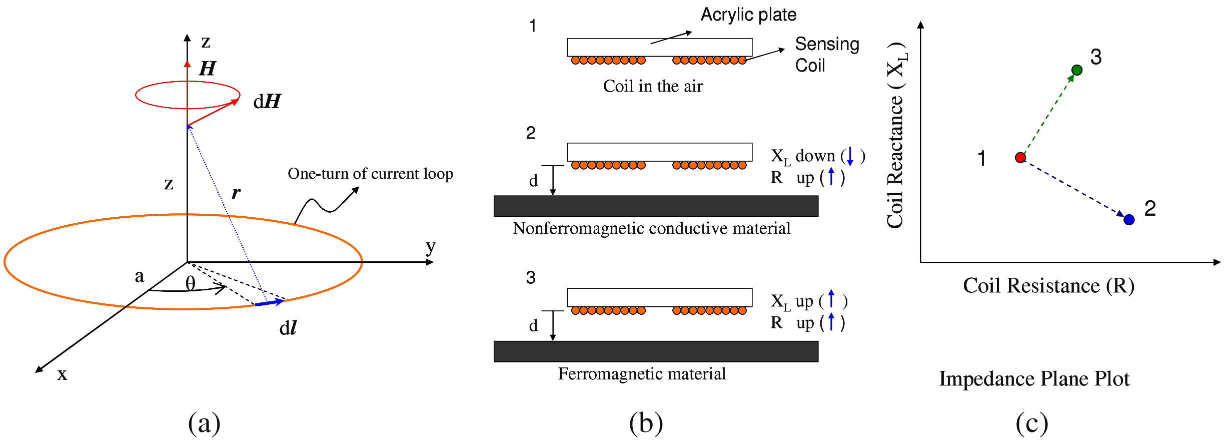

Figure 1. Principle of operation for the sensor: (a) magnetic field intensity along the axis of coil; (b) flat coil in air, and placed over non-ferromagnetic conductive and ferromagnetic materials, with changes in inductive reactance and resistance shown; (c) impedance plot of the coil. Parts (b) and (c) are redrawn from [14].

They found that the relationship was approximately linear for small ranges of coil-to-target distance, such as a range of 0.4–0.8 mm, and they obtained a resolution of better than 0.5 μm in submicrometer displacements. However, it is notable that over a larger range of coil-to-target distances, the relationship between the oscillator frequency and distance is nonlinear. Kejik *et al* also suggested a low-cost inductive proximity sensor, and studied temperature compensation for the sensor output [10]. However, to the best of our knowledge, studies about inductive sensors for monitoring vibration have been scarce; one such study is a work by Mavroyannakis *et al* [11]. Recently, the authors demonstrated promising results using an inductive sensor for vibration monitoring [12]. The previous inductive vibration (IV) sensor used a frequency-to-voltage converter IC and an analog-to-digital converter for crack detection in a vibrating conductive beam. The work was the first reported application of an inductive sensor to the vibration monitoring of cracked beam structures. Although several commercial eddy current sensors are available for vibration monitoring, they need complicated electronic interface circuits and signal processing; this makes them expensive.

In this paper, we simplify the electromagnetic field-based (EFB) vibration sensor further and propose a novel sensing technique that can efficiently measure the dynamic displacements of general conductive or ferromagnetic objects under resonant fatigue testing. The novelties of the proposed sensor include a significantly simplified sensor electronic interface circuit compared to the previous version [12] and an efficient timer counting method for monitoring high-frequency vibrations. The prototype of the electromagnetic field-based (EFB) vibration sensor consists of a coil, an electronic oscillator circuit, a microprocessor, and a high-performance digital-to-analog converter. It provides noncontact measurement of vibrations up to 5 kHz, as long as the displacement amplitudes are large enough to be detectable. In the following sections, the operating principle of the EFB sensing mechanism is described, and the configuration of the sensor components is given. To demonstrate the sensor's performance, a series of basic verification tests and a calibration test have been conducted using specimens made of AISI 100 carbon steel and Al 6061–T6 aluminum alloy.

2. Sensing mechanisms of the electromagnetic field-based sensor

The key component of the proposed EFB sensor is a flat-form coil whose impedance changes with distance from a conductive or ferromagnetic test specimen. Any coil has both resistance R and inductance L; assuming that the capacitance of the coil is negligible, the coil has a total impedance of $Z = \sqrt{(X_L)^2 + R^2}$, where the inductive reactance $X_L = 2\pi f L$ depends on the frequency f of the signal applied to the coil and the coil's inductance L. The resistance is determined by the length, cross-sectional area, and material of the wire. The effective inductance L_{eff} of a coil of general shape with N turns is approximately [13]:

$$L_{\text{eff}} = \frac{\mu N \int\int H \, \mathrm{d}A}{I} \qquad (1)$$

where μ is the magnetic permeability of the material surrounding the coil through which the magnetic field travels, I is the current through the coil, H is the magnetic field strength, and the integration is over the perpendicular area A through which the magnetic field travels. The proposed sensor uses the principle that as conductive and ferromagnetic objects approach the coil, the inductance L_{eff} and therefore the impedance of the coil change due to changes in the magnetic permeability of the material near the coil and the magnetic field strength.

As shown in figure 1, in isolation (i.e., when air-cored) the coil has constant inductive reactance and resistance. However, if the coil is brought in proximity to a ferromagnetic material, part of its core is replaced with a material of significantly higher magnetic permeability than air, and as a result the inductance L and inductive reactance X_L increase. If an air-cored coil that is being driven with an AC current is brought close to a conductive but non-ferromagnetic material,

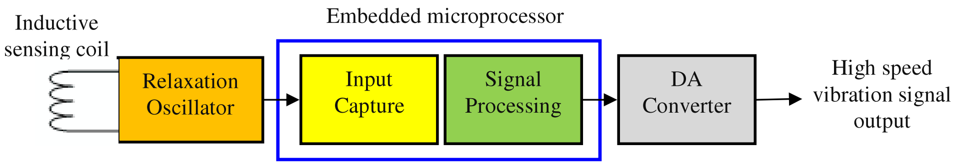

Figure 2. Hardware configuration of the noncontact EFB vibration sensor.

the changing magnetic field around the coil induces an eddy current in the conductive material, and this eddy current in turn induces an additional magnetic field that opposes the original one, effectively reducing the magnetic field strength. The net effect is to reduce the rate of change of the magnetic flux, thereby reducing the coil's effective inductance. When brought close to either ferromagnetic or conductive specimens, the resistance of the coil increases [14]. It is the change in the coil's impedance that the proposed sensor uses to detect the vibration of ferromagnetic and conductive test specimens. The amount of change depends on the distance to the specimen and material parameters, as well as the frequency at which the coil is excited.

Trial and error tests were used to determine the most appropriate coil geometry. The coil is air-cored. A flat-form geometry was determined to be most sensitive to the vibration of our test specimens. The magnetic field intensity is reduced with distance from the coil, and a flat-form geometry allows the specimen to get close to the stronger parts of the field.

3. Electromagnetic field-based vibration sensor

A schematic of the hardware configuration of the proposed sensor is shown in figure 2. It consists of an inductive coil, electronic circuitry that generates oscillations at a frequency that depends on the coil's impedance, an embedded microprocessor module that converts frequencies to digital signals, and a high-performance digital-to-analog converter that produces the final analog sensor output. Key technologies used for the proposed novel vibration sensor are (1) a timer counting method using the input capture function and timer of the embedded microprocessor module and (2) significant simplification of the analog circuitry for producing oscillations. The circuit is significantly simpler than the previous version [12], and is more robust to noise because the noise-prone frequency-to-voltage (FV) converter and operational amplifier have been eliminated.

3.1. Principle of operation of the relaxation oscillator

The relaxation oscillator shown in figure 3 is proposed for producing a signal whose frequency of oscillation depends on the effective impedance of the sensing coil. In each cycle, the rising and falling parts of the oscillation are produced by first charging the capacitor $C4$, and then discharging it; the bipolar junction transistor Q turns off and on to switch the circuit between its rising and falling phases. When the transistor Q is off, the output voltage V_0 rises in a way that is dominated by a single time constant that involves both the circuit's resistor

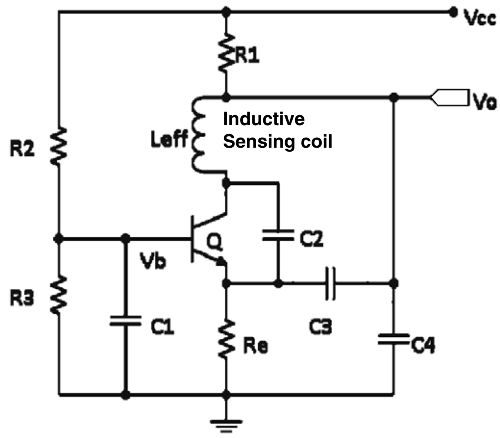

Figure 3. Schematic of the relaxation oscillator circuit.

and capacitor components and the effective impedance of the sensing coil, such that when the effective impedance increases, the rise time decreases. On the other hand, when Q is on, the charge stored on $C4$ is discharged; the time constant for the discharge again involves the effective impedance of the sensing coil. Whether the transistor Q is off or on is determined by the voltage V_b, which also oscillates. In the rising direction, the voltage V_b charges with time constant $\tau = R2 \times C1$; once Qs base-to-emitter voltage exceeds the cut-on voltage of the transistor, Q turns on. This in turn causes the voltage V_b to drop, as Qs base current slowly discharges $C1$. At the same time, there is a current in resistor Re as the capacitor $C4$ discharges; this current serves to reduce the base-to-emitter voltage of Q, tending to turn the transistor off again. Repetitive operations of these cycles generate the relaxation oscillation frequencies.

The base oscillation frequency, or the frequency when the sensor is not near a specimen, can be adjusted by choosing different values for the resistor and capacitor components. As ferromagnetic material approaches the coil, the impedance of the coil increases; this results in faster rise and fall times for the output voltage, and therefore an increase in frequency of oscillation from the base frequency. The component values used in the experimental work presented in this paper are given in table 1. The component values were chosen to give a base oscillation frequency of 5 kHz; the oscillation frequency increases to 11 kHz when the coil is the minimum allowable distance of 2.5 mm from our (ferromagnetic) carbon steel specimen. Figure 4 is the output of the relaxation oscillator as captured from an oscilloscope when the carbon steel specimen is 2.5 mm from the coil. It shows an oscillation of 5.49 kHz.

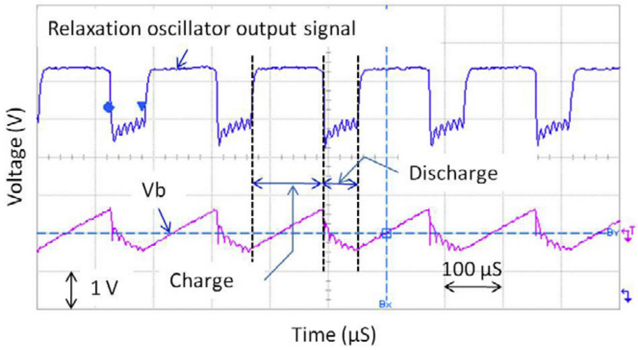

Figure 4. The output of the relaxation oscillator and voltage V_b when the carbon steel specimen is 2.5 mm from the sensing coil.

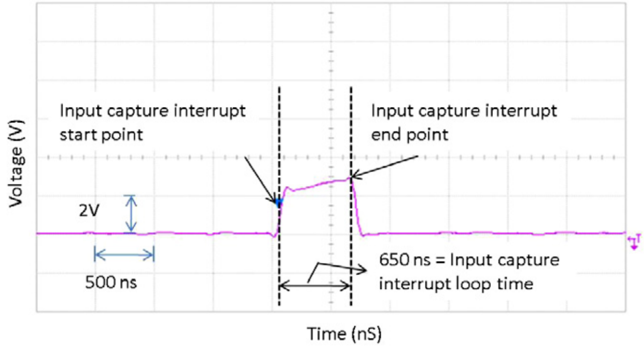

Figure 5. Time required to process a single input capture interrupt.

Table 1. Values of circuit components in the relaxation oscillator for the prototype EFB vibration sensor.

Device		Values
Resistors	$R1$	2 kΩ
	$R2$	20 kΩ
	$R3$	30 kΩ
	Re	470 Ω
Capacitors	$C1$	0.001 μF
	$C2$	220 pF
	$C3$	0.001 μF
	$C4$	0.01 μF
Inductor	L^a	16.8 μH

[a] The inductor was measured using an EDC-1630 digital LCR meter.

3.2. Novel timer counting method for sensing vibration

The frequency produced by the relaxation oscillator is inversely related to the distance to the target specimen. The proposed method does not use the analog-to-digital converter (ADC) of the embedded microprocessor to capture the oscillation, and so avoids the problems associated with noise when capturing analog signals using an ADC. Instead, the output of the relaxation oscillator is given to the input capture unit of the embedded microprocessor; it is notable that the functionality of the input capture provides an efficient method for measuring the period or pulse width of signals. In the proposed implementation, each time the rising oscillating signal passes a threshold, an input capture interrupt is triggered. On the interrupt, the count value of a timer in the microprocessor is first copied and then reset; the timer then counts at the microprocessor's clock frequency. The timer counts the clock cycles until the next interrupt occurs, thereby counting the microprocessor clock cycles in one period of oscillation. The most recent timer count value copied is a digital signal that is inversely related to the current oscillation frequency of the output of the relaxation oscillator.

For the implementation of the proposed EFB vibration sensor, a dsPIC33FJ128GP206 embedded microprocessor module was used. Either of two 16-bit timers (timer 2 and timer 3) can be selected for the input capture channel. A linear relationship was observed between the frequency of oscillation of the relaxation oscillator (expressed in hertz) and the timer count for the range of frequencies used in the relaxation oscillator. Considering that the microprocessor clock speed is 40 MHz, recorded counts represent time to the nearest 25 ns. This limits the resolution of the frequency measurement. The worst-case error in frequency measurement is when the oscillation frequency is highest.

Another important consideration is how long the embedded microprocessor takes to respond to the input capture interrupt and run the interrupt service routine that resets the timer, setting the counting into motion. This time is overhead in the period detection method, and is a limiting factor in how high-frequency an oscillation the proposed EFB sensor can detect. The time was measured experimentally by setting a digital output for the duration of the interrupt service routine. Figure 5 shows this digital output as captured on the oscilloscope; as shown in the figure, the required time for the triggering and resetting process is 650 ns. This is deemed sufficient to detect the high-frequency vibration of materials.

The implementation was verified by comparing the frequency of the relaxation oscillator's output as measured by the embedded microprocessor module with the frequency as measured directly using an oscilloscope. Figure 6 shows the oscilloscope trace when the proposed sensor is in close proximity to the same carbon steel specimen used in figure 4, but at a slightly different distance; the measured frequency is 5.49 kHz. At the same time, the microprocessor's timer count value was 7277 ($0x$1C6D), which corresponds to a period of 7277×25 nS $+$ 650 nS $=$ 182.575 μS, for a matching calculated frequency of $1/182.575$ μs $=$ 5.477 kHz.

The timer count is periodically converted to an analog signal using a high-performance digital-to-analog converter. The digital-to-analog converter used is the high resolution and high-speed AD569, with a 16-bit monotonic voltage input and a 3 μs conversion time; the conversion time affects the rate at which the sensor output can be updated. The analog signal is the output of the EFB vibration sensor, and represents the distance between the coil and targeted conductive or ferromagnetic object. With this method, we saw significantly less noise than with the previously reported method [12]. The base oscillation frequency can be made easily adjustable by the user by replacing resistor $R1$ with a potentiometer. Experimentally, a base oscillation frequency of 5 kHz was found to be most appropriate.

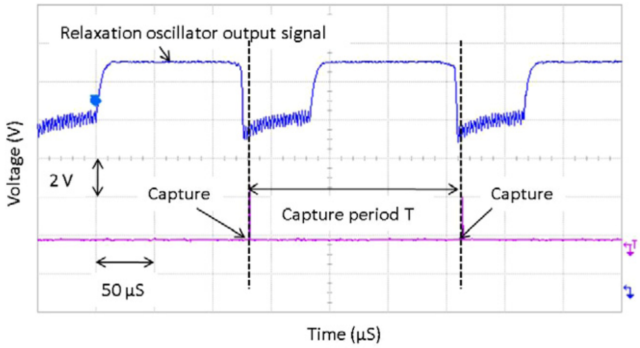

Figure 6. Relaxation oscillator output and corresponding input capture signal, as measured on an oscilloscope.

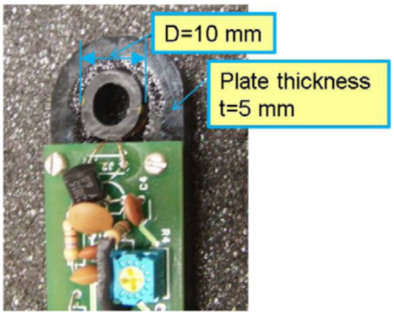

Figure 8. Fabricated sensing coil.

4. Fabrication of the sensing coil

A sensing coil was fabricated and tested for this study. The coil has forty turns, with detailed dimensions as shown in figure 7. Figure 7 also shows a computation of the approximate coil inductance, using an equation from [15]. The sensing coil was fabricated by hand, using copper wire coated with enamel, a plastic tube, an acrylic plate, and soft transparent glue sticks. First, a groove was made around the outer circumference of the plastic tube. The copper wire was wound around the tube, seated in the groove. In this way, the plastic tube is part of the core of the coil. A hole was drilled in an acrylic plate of thickness slightly less than the length of the plastic tube. The tube with the coils was inserted into the hole and attached to the acrylic plate using the glue. A photograph of the manufactured sensing coil, annotated with dimensions, is given in figure 8.

The prototype sensor was designed and built modularly, in three parts: (1) sensing module; (2) computing module and (3) power module. The sensing module consists of the sensing coil and the relaxation oscillator circuit. The computing module consists of a microprocessor board (dsPIC33FJ128GP206) and a high-speed D/A converter (AD569), mounted together on a printed circuit board. Software, written in C and running on the microprocessor, implements the timer counting method previously described to monitor vibrations. The power module converts AC power to 12 V DC power to provide power to the computing module. As shown in figure 9, the three modules are integrated in a three-layer rugged design that includes a cable with a BNC connector, for convenient connection to a data acquisition system.

5. Experimental testing and results

The primary experimental demonstration of the prototype EFB vibration sensor focuses on verification of its sensing capabilities, and reveals the inter-relationships among displacement, analog voltage output and frequency of vibrating target specimens for different conductive materials. As is also the case with other EFB sensors, including eddy current sensors, the

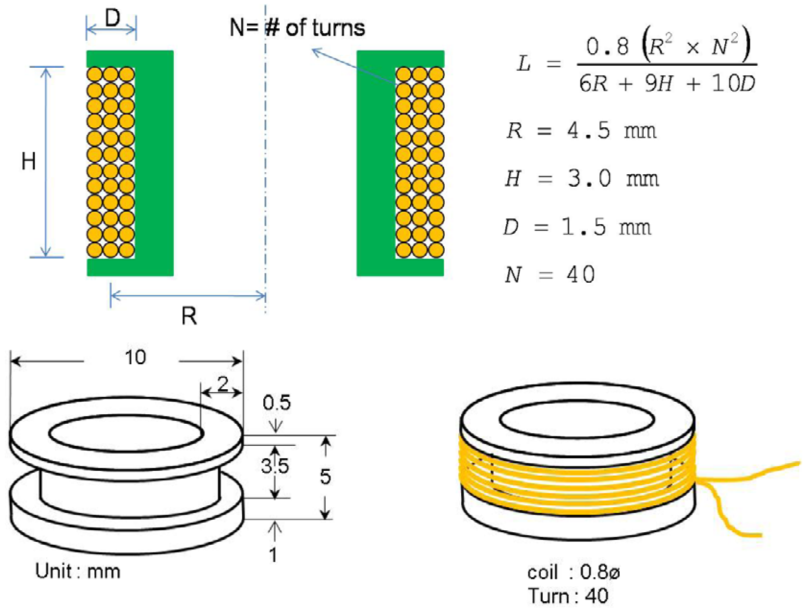

Figure 7. Detailed dimensions of the fabricated sensing coil, and Wheeler's approximation of inductance for a multi-layer air-cored coil [15]. (Note: calculated inductance is 14.97 μH; measured inductance is 16.8 μH.)

Table 2. Specimens used for testing of EFB vibration sensor.

	Length (inch)	Thickness (inch)	Material	Characteristics
Specimen 1	Total length = 4.2 Length of cantilever = 3.675	0.071	AISI 1095 steel	Ferromagnetic; conductive
Specimen 2	Total length = 4.0 Length of cantilever = 3.475	0.071	Al 6061–T6 aluminum	Non-ferromagnetic; conductive

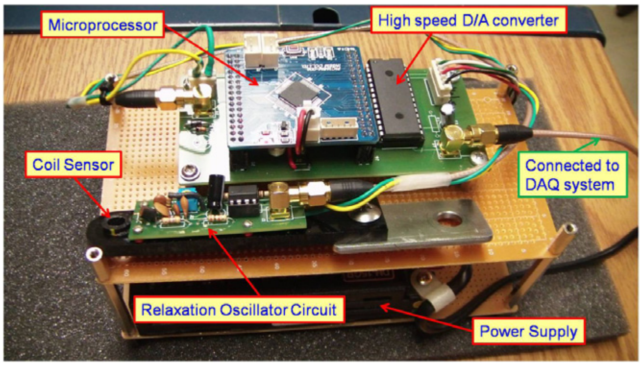

Figure 9. Modularized EFB vibration sensor.

displacement amplitudes that can be sensed and the appropriate near gap (defined in figure 13(a)), or distance between the coil and the target specimen, are important factors that are determined by, among other things, the geometric dimensions and the number of turns of the coil, and the size and material properties of the target specimen. The effects of these factors on the sensing capability have not been fully addressed in this paper; the focus of this work is the new EFB vibration sensing method itself.

In the verification test, amplitude-controlled fatigue tests are conducted using a closed-loop resonant fatigue testing system. The testing system uses feedback supplied from a scanning laser vibrometer to control the displacement amplitude. The proposed EFB vibration sensor is used to monitor the vibrations, and its measured displacements are verified using an independent measurement from the scanning laser vibrometer. The results are used to understand the relationships among the displacement, the voltage output from the EFB vibration sensor and the vibration frequency.

5.1. Test specimens

Two cantilevered specimens made specifically for giga-cycle resonant fatigue testing were chosen as target specimens. Their geometrical dimensions and detailed specifications are summarized in table 2 and figure 10. Specimen 1, of (ferromagnetic and conductive) AISI 1095 carbon steel, is 4.2 inches long, 0.2 inches wide, and 0.071 inches thick. Specimen 2, of (non-ferromagnetic and conductive) Al6061–T6 aluminum alloy, is 4.0 inches long, 0.2 inches wide, and 0.071 inches thick. Both specimens are attached to fixtures made of titanium 6–4 alloy. The operating deflection shape of the specimens was measured, and it was found that the peak displacement occurs at the tip of the specimens at the first two natural frequencies. Thus, the displacement is always measured at the cantilever tip. To increase the intensity of the reflected laser beam for the laser vibrometer, reflective film was attached to the front surface of the tip of each specimen.

5.2. Experimental test configuration

The overall test configuration is illustrated in figure 11. The closed-loop resonant fatigue test system used consists of an electrodynamic shaker (DataPhysics V100), an amplifier (DataPhysics SS1000T), a DataPhysics ABACUS DAQ chassis and a scanning laser vibrometer (Polytec Scanning Vibrometer-400-M2-20). The test system is designed to search for the resonant frequency of the specimen, and dwell at the identified frequency while maintaining the targeted displacement amplitude with control feedback from the scanning laser vibrometer. However, the current verification test did not use the resonant search test capability; instead, a dwell test was conducted with the specimen vibrating at multiple operator-defined frequencies with predetermined displacement amplitudes. In the dwell test, the test system shakes the specimen at predetermined frequencies, while using control feedback from the scanning laser vibrometer to maintain the predetermined displacement amplitude. A portable NI DAQ unit (NI-USB-6251) and a laptop computer were used to acquire both the analog voltage output from the EFB sensor and velocities from the scanning laser vibrometer. In real resonant fatigue tests, the EFB sensor can also provide feedback signals to the controller system in the same test configuration used in this paper. A photograph of the laboratory test setup and equipment is given in figure 12.

5.3. Amplitude-controlled verification test

In this test, steady-state displacements were measured using the EFB vibration sensor during dwell tests for the two specimens at a number of vibrating frequencies. Specimen 1 was tested at four frequencies: 30, 100, 200, and 1100 Hz. Specimen 2 was tested at four frequencies: 30, 100, 200, and 1290 Hz. It should be noted that it requires less power to achieve the desired displacement amplitude at resonant frequencies of the specimen than it does at non-resonant frequencies. The achievable displacement at higher frequency is limited due to shaker power limits. The near gap was set to either 0.065 or 0.020 inch, depending on the vibrating frequency; a smaller gap was used at higher frequencies, when displacement was limited. The near gap was chosen based on the quality of the measured response. In general, the low and upper limits of the near gap for electromagnetic type sensors vary depending on the size of sensing coil and specimens. A diagram showing the displacement amplitude (d_{pk-pk}) and near

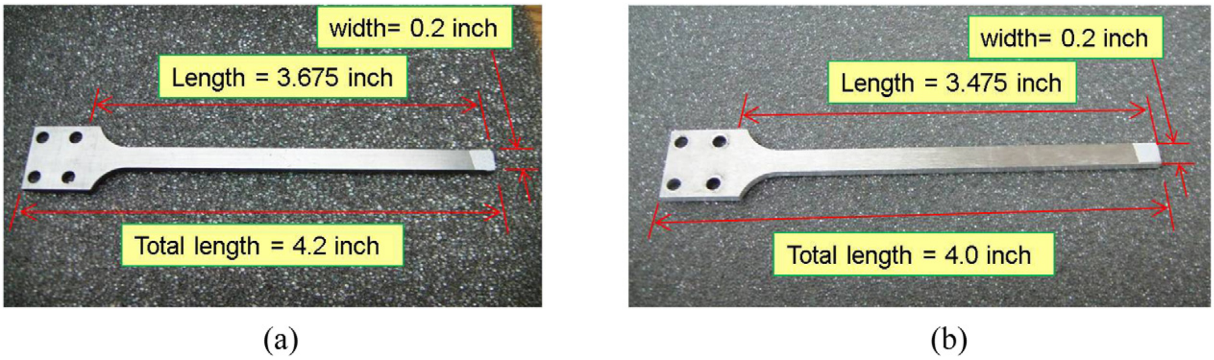

Figure 10. Dimensions of target specimens: (a) specimen 1 (AISI 1095 carbon steel), and (b) specimen 2 (Al 6061–T6 aluminum alloy).

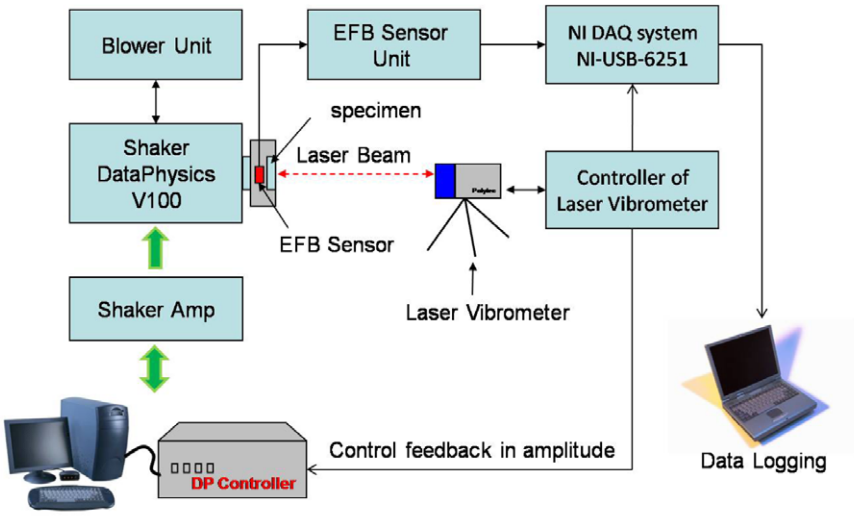

Figure 11. Experimental test configuration integrating of a scanning laser vibrometer and shaker controller for closed-loop giga-cycle resonant fatigue testing.

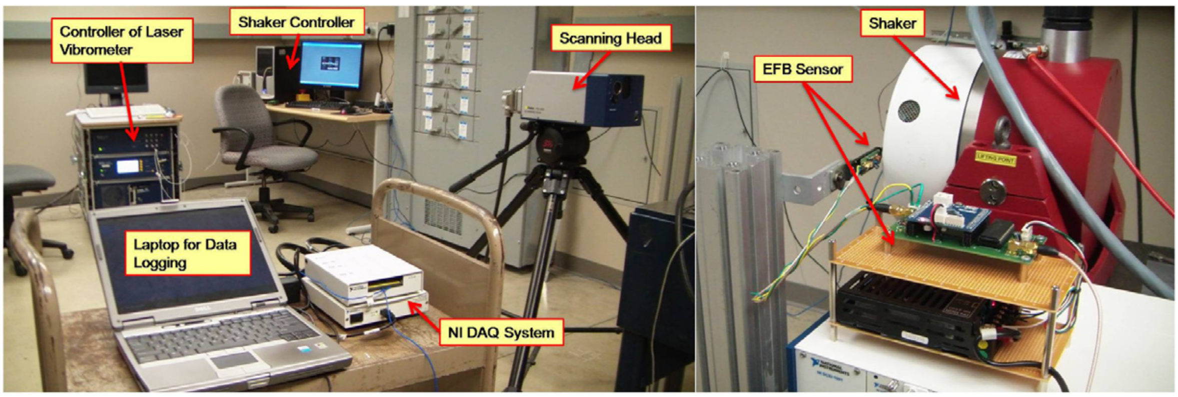

Figure 12. Experimental test setup and configuration for EFB vibration sensor verification test.

gap (d_0) is given in figure 13(a). Figure 13(b) shows a typical test, in this case for specimen 1 vibrating at 30 Hz with a 2.0 mm $d_{\mathrm{pk-pk}}$ and a near gap of 0.065 inches.

5.3.1. Test with specimen 1—AISI 1095 carbon steel. The first two natural frequencies of specimen 1 are 194 and 1180 Hz. The near gap (d_0) was set to be 0.065 inch at 30, 100 and 200 Hz and 0.020 inch at 1100 Hz. The output of the EFB vibration sensor was sampled at a rate of 10 kHz for the tests at the three lower frequencies; for the 1100 Hz test, the sensor output was sampled at 40 kHz. Figure 14 shows the voltage at the output of the EFB vibration sensor as a function of time for a 30 Hz test, at a variety of displacement amplitudes. As the displacement amplitude decreases, the voltage output also

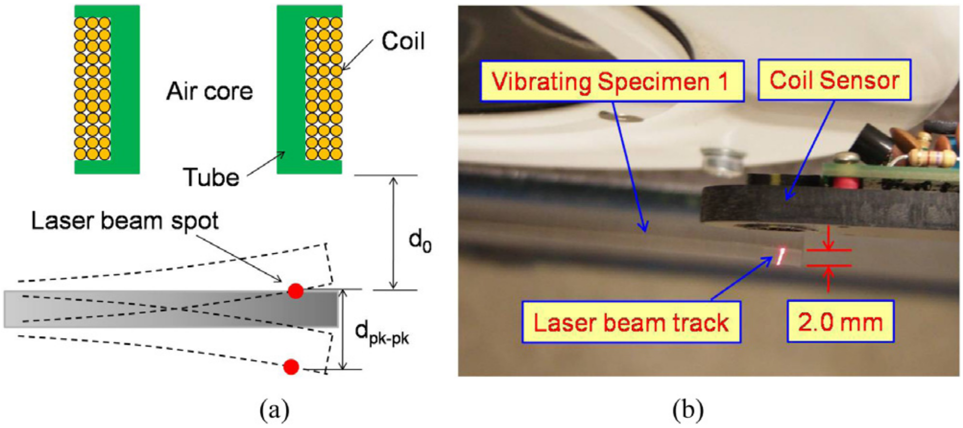

Figure 13. (a) Near gap (d_0) and displacement amplitude (d_{pk-pk}) and (b) specimen 1 vibrating at 30 Hz with $d_{pk-pk} = 2.0$ mm and $d_0 = 0.065$ inch.

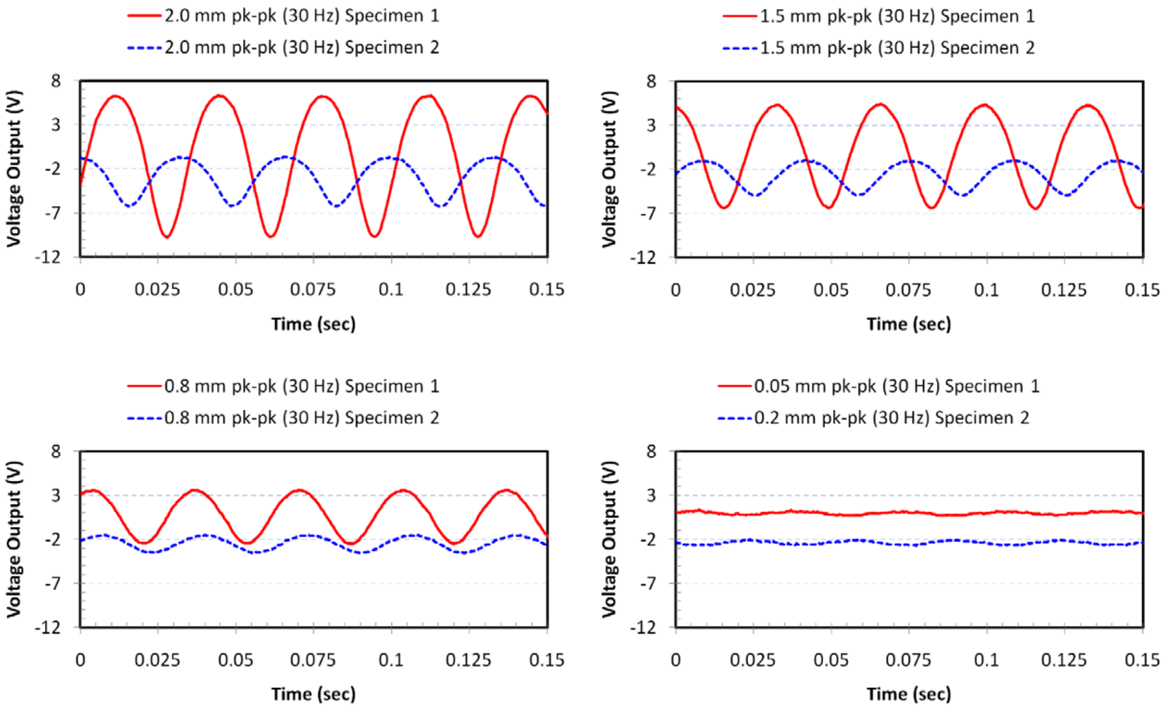

Figure 14. Outputs from EFB sensor from tests with specimen 1 (AISI 1095 carbon steel) and specimen 2 (Al 6061–T6 aluminum alloy) vibrating at 30 Hz with near gap (d_0) of 0.065 inch.

proportionally decreases. The results show that the proposed EFB sensor is capable of sensing the low-frequency vibration. In further tests not shown in this paper, it was found that the EFB sensor could measure displacements with amplitudes as low as 20 μm. Figures 15 and 16 show similar EFB sensor output voltages for tests using higher frequency vibrations, at 100 and 200 Hz.

At a vibration frequency of 1100 Hz, noise was significant. At higher frequencies, the signal is smaller, so that noise becomes comparable in magnitude to the signal. Environmental effects such as movement of the heavy duty table used for the test setup were also a factor. To mitigate the noise, a high pass filter with a cut-off frequency of 900 Hz was used to process the sampled data. Although this filtering will attenuate the vibration frequency in addition to the noise, the approach is reasonable because the test specimen is under resonant vibration and we are aiming simply to verify that the EFB vibration sensor is capable of capturing vibrations at higher frequencies. Figure 17 shows the sensor voltage output as a function of time when specimen 1 vibrates at 1100 Hz. Displacement amplitudes as small as 4 μm can be observed.

5.3.2. Test with specimen 2—Al 6061–T6 aluminum alloy. Specimen 2 is made of Al6061–T6 aluminum alloy, which is conductive but non-ferromagnetic. The first two natural frequencies of specimen 2 were found to be 223 and 1360 Hz. The near gap (d_0) was set to be 0.065 inch at 30, 100, and 200 Hz and 0.020 inch at 1290 Hz. The output of the EFB

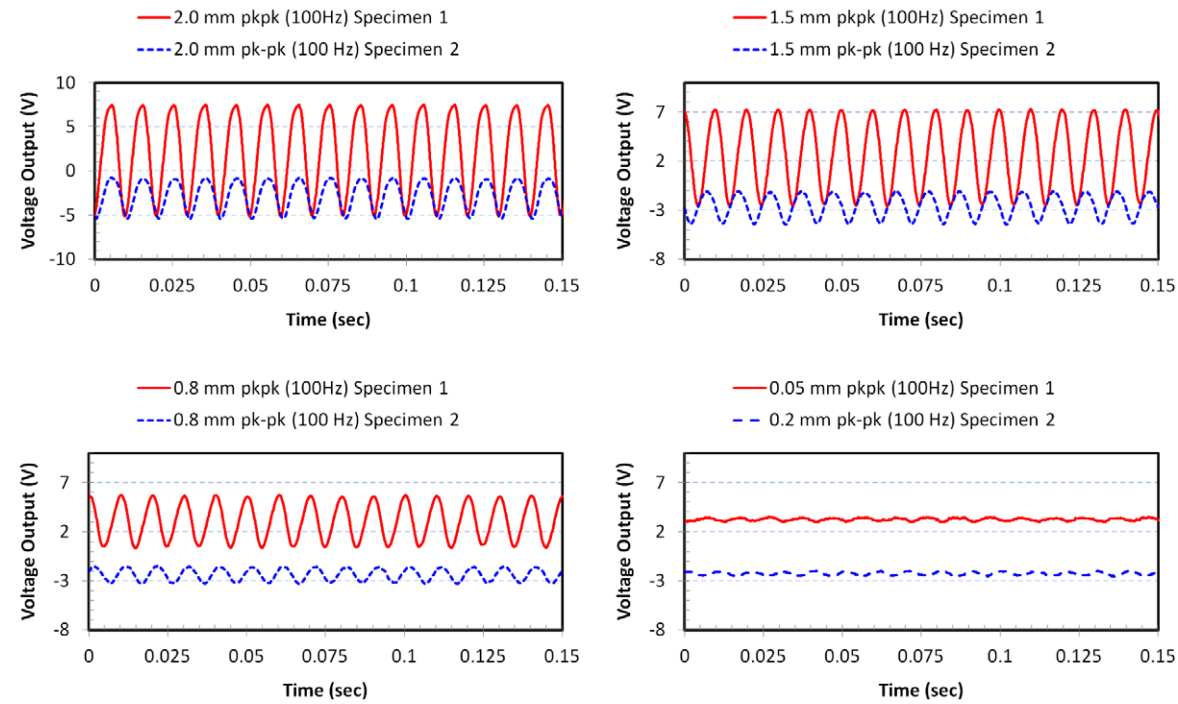

Figure 15. Outputs from EFB sensor from tests with specimen 1 (AISI 1095 carbon steel) and specimen 2 (Al 6061–T6 aluminum alloy) vibrating at 100 Hz with near gap (d_0) of 0.065 inch.

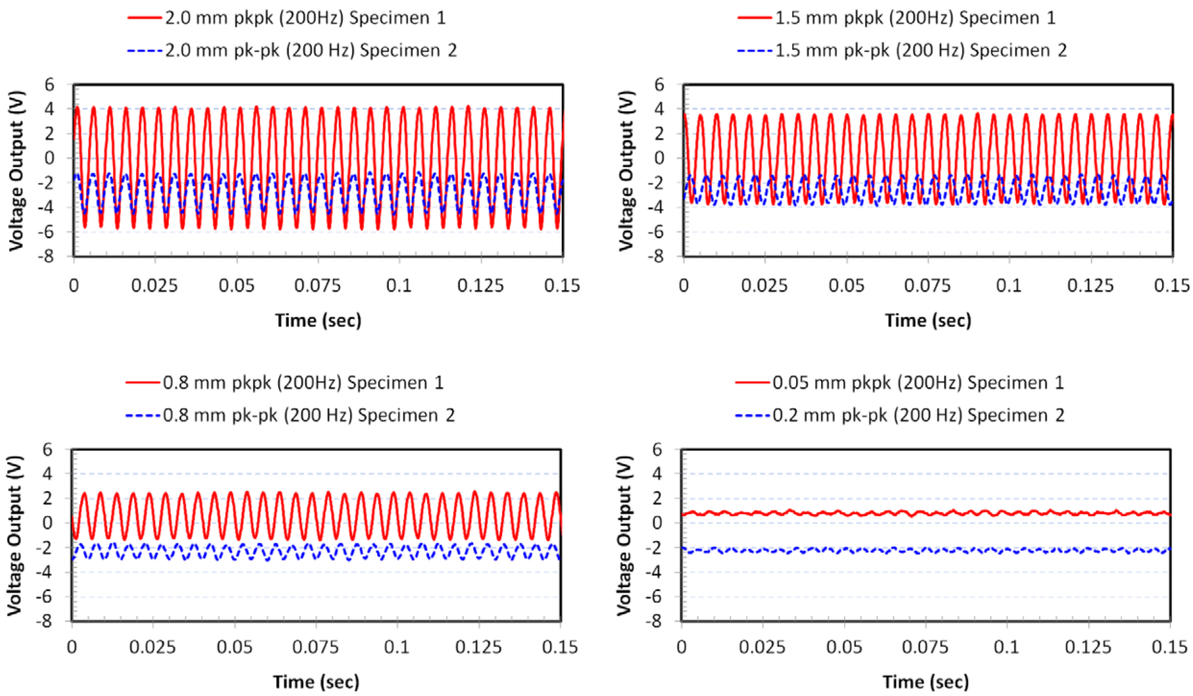

Figure 16. Outputs from EFB sensor from tests with specimen 1 (AISI 1095 carbon steel) and specimen 2 (Al 6061–T6 aluminum alloy) vibrating at 200 Hz with near gap (d_0) of 0.065 inch.

vibration sensor was sampled at a rate of 10 kHz for the tests at the three lower frequencies; for the 1290 Hz test, the sensor output was sampled at 40 kHz. As before, a high pass filter with cut-off frequency 1100 Hz was used to process the sampled data for the 1290 Hz test, in order to mitigate the effects of noise. These test conditions were intentionally chosen to match those of the tests of specimen 1, so that the results can be more directly compared.

Figures 14–17 show the sensor voltage output as a function of time for experiments at the different frequencies, with a variety of displacement amplitudes. From the results, it is clear that the EFB vibration sensor can also

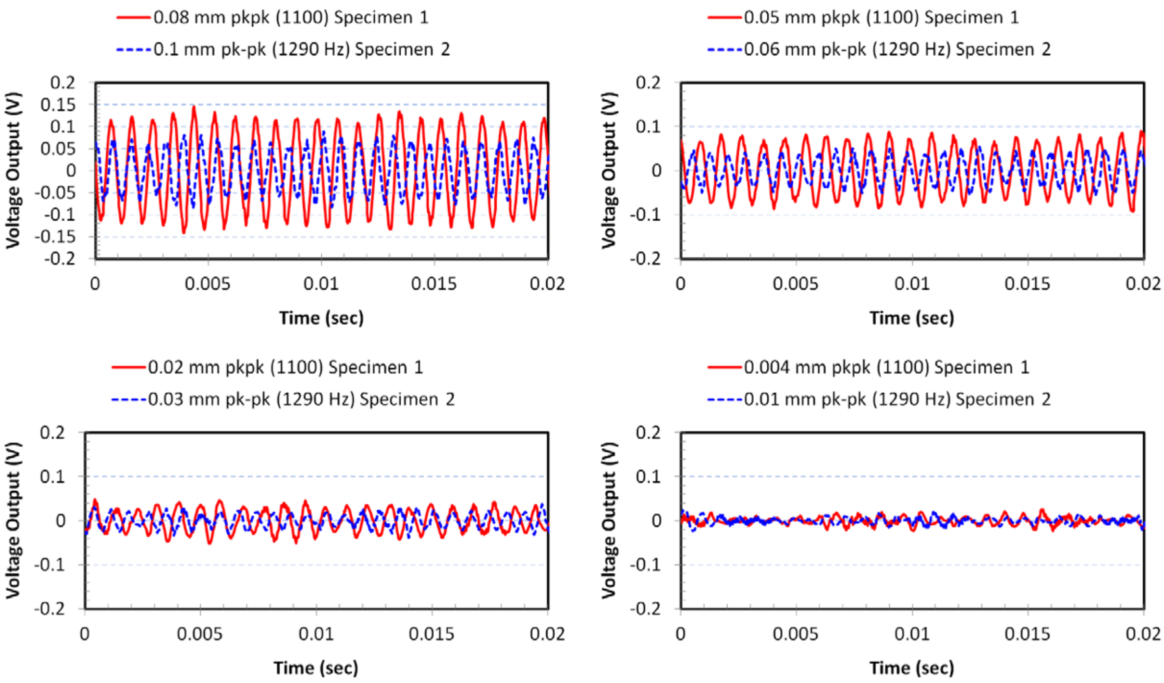

Figure 17. Outputs from EFB sensor from tests with specimen 1 (AISI 1095 carbon steel) specimen 2 (Al 6061–T6 aluminum alloy) vibrating at 1100 and 1290 Hz, respectively with near gap (d_0) of 0.020 inch.

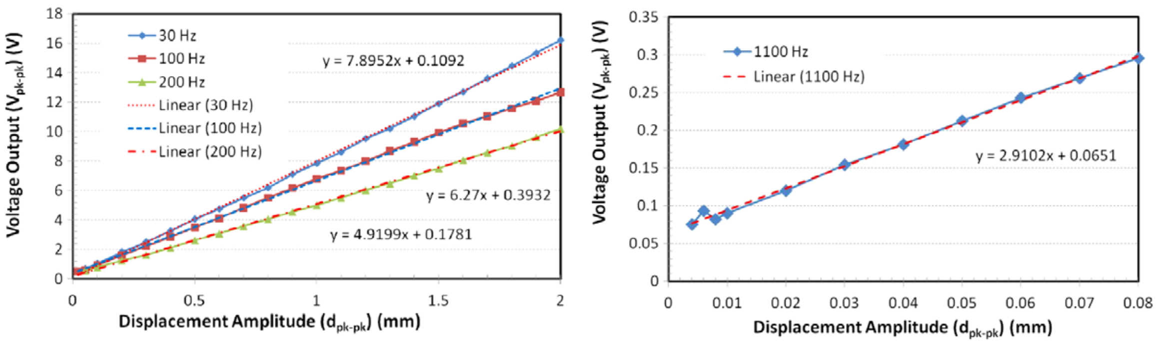

Figure 18. Calibration curves for specimen 1 (AISI 1095 carbon steel) at 30, 100, 200 and 1100 Hz vibration frequencies.

effectively measure dynamic displacements of the aluminum alloy specimen. Compared to the responses for the carbon steel specimen, the responses for the aluminum alloy specimen show much lower peak-to-peak amplitudes in the sensor output voltage. As a result, the minimum displacement amplitude measurable is smaller for carbon steel than for aluminum alloys.

5.4. Relationship of displacement amplitude, frequency and sensor output

The proposed EFB vibration sensor is intended to measure physical displacements of the vibrating specimen under resonant fatigue testing. Thus, it is important to understand the relationship between the sensor output voltage and the physical displacement. A series of experiments were conducted to investigate the relationship, by mapping the sensor output voltage to physical displacement measured independently using the scanning laser vibrometer. The test results show that displacement is related approximately linearly to the sensor output voltage over the range of displacements tested. However, the linear proportionality constant depends on the frequency of vibration, and the specimen used. It is notable that the linear relationship between displacement and sensor output voltage holds for displacements of up to 2 mm in this study.

Figure 18 shows plots of the EFB vibration sensor voltage output as a function of the independently measured displacement amplitude for the series of tests that use specimen 1. Linear regression was used to find the best mapping for each vibration frequency; the mathematical equations for the best fit lines are annotated on the figures. As the vibration frequency increases, the slopes of the linear calibration curves are observed to gradually decrease; over the

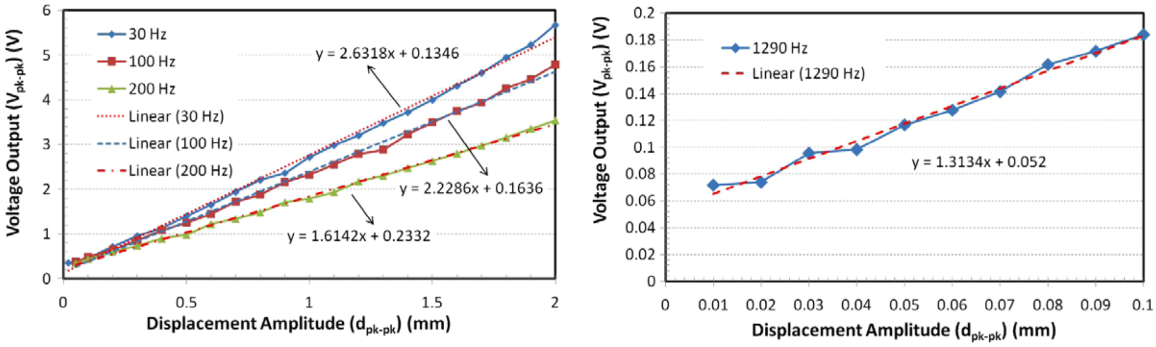

Figure 19. Calibration curves for specimen 2 (Al6061–T6 aluminum alloy) at 30, 100, 200 and 1290 Hz vibration frequencies.

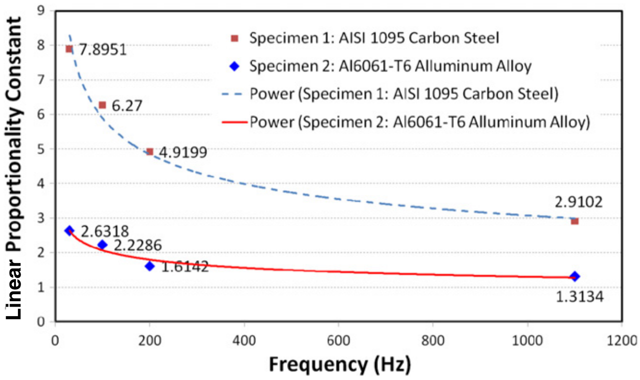

Figure 20. Linear proportionality constants of regressed curves versus frequency for specimen 1 (AISI 1095 carbon steel) and specimen 2 (Al6061–T6 aluminum alloy).

range of frequencies tested, the linear proportionality constant decreased from 7.8951 to 2.9102.

Figure 19 shows the results of similar tests for specimen 2. Also shown are the linear relationships between sensor voltage output and displacement amplitude. The proportionality constants for specimen 2 are considerably smaller than those for specimen 1.

The linear proportionality coefficients for a given specimen are plotted versus the excitation frequencies in figure 20. A power law relationship is found to exist between the linear proportionality constant and the frequency. As shown in figure 20, the linear proportionality constants asymptotically approach positive values as the vibration frequency increases. This supports the claim that the EFB vibration sensor can measure vibrations at higher frequencies, as long as the displacement amplitude is sufficiently large to be measured. Theoretically, the EFB vibration sensor should be able to measure the vibrations at frequencies up to those that can be resolved using the proposed timer counting method; for our implementation, which can resolve a minimum time period of 675 ns, it should be possible to measure vibrations at frequencies up to 1.48 MHz. However, the measurement of vibrations at these frequencies has not been verified in this study because of the unavailability of a shaker having sufficient power.

5.5. Effects of vibration frequencies on response output of EFB vibration sensor

To investigate the frequency-dependent characteristics of the EFB sensor, broadband uniformly random signals were loaded to the shaker. For this test, the EFB sensor was positioned to measure dynamic movement of the armature of the shaker which is made of carbon steel. The data were sampled at 20 kHz. As expected, the power spectrum of the voltage output from the EFB sensor has a non-uniform envelope. Inspecting the envelope of the EFB sensor power spectrum along the initial frequency range, the magnitudes of the power spectrum seem to be decreasing by a power law as observed in figure 20. To remove unnecessary dynamics from the shaker and the table, the same power spectra were measured under ambient noise signals. The EFB sensor indicated a strong frequency-dependent power spectrum even under the ambient noise excitation signals again. From these tests, the proposed noncontact EFB sensor is considered to be suitable for single-frequency applications such as monitoring of resonant fatigue testing as meant in this paper. However, if the demonstrated frequency-domain response is fully characterized, the frequency-dependent response output from the EFB sensor can be potentially calibrated. Thus, the noncontact EFB sensor is potentially considered as an effective sensor for monitoring the vibration of structures subjected to ambient excitations.

6. Summaries and conclusions

In this paper, a novel sensing technique for a noncontact electromagnetic field-based (EFB) vibration sensor has been presented to monitor the health of conductive specimens under resonant fatigue testing. The sensor is based on a relaxation oscillator whose oscillation frequency changes according to the distance to the target specimen. Specifically, the frequency produced by the relaxation oscillator is inversely related to the distance to the target specimen. This is because the distance between the sensing coil and the targeted specimen causes a change in the impedance of the sensing coil. Sensor interface electronics consist of the relaxation oscillator, an embedded microprocessor module, and a high-speed digital-to-analog converter. For sensing the dynamic response of conductive objects, key technologies are proposed: (1) a timer counting method using the input capture functionality and timer of the embedded microprocessor module which has a sampling resolution of 675 ns including the required time for triggering and resetting and (2) significant simplification of the analog circuitry, with less noise than a previously published version [12].

A prototype EFB vibration sensor was fabricated, including a hand-made sensing coil. To verify the performance of the sensor, carbon steel (ferromagnetic and conductive) and aluminum alloy (non-ferromagnetic and conductive) cantilever specimens were tested under single-frequency sinusoidal excitations, for a variety of frequencies and displacement amplitudes. The analog voltage outputs from the EFB vibration sensor were measured. In the verification test, a closed-loop amplitude-controlled fatigue testing system was utilized, where a scanning laser vibrometer provides displacement feedback to the shaker controller system. Summarizing the experimental observations and conclusions,

(1) The voltage output from the EFB vibration sensor was found to be linearly proportional to the displacement amplitude of the specimens. This implies that the EFB vibration sensor is suitable for the measurement of dynamic displacements of conductive materials. Linearity was observed for both AISI 1095 carbon steel and Al6061–T6 aluminum alloy specimens.
(2) The EFB vibration sensor could measure single-frequency vibrations with amplitudes of as little as 4 μm for the carbon steel specimen, and 10 μm for the aluminum alloy specimen.
(3) The sampling resolution of the timer counting method implemented on the embedded microprocessor is sufficiently high enough to sense changes in frequency of the relaxation oscillator. In addition, the conversion of the D/A converter is fast enough to capture high-frequency vibration.
(4) However, it was found that the relationship between the sensor output voltage and the physical displacement is highly dependent on the excitation frequency. According to the verification tests, the linear proportionality constants were observed to asymptotically reduce to lower bounds corresponding to positive values, as the frequency was increased. This suggests that the EFB vibration sensor can measure high-frequency vibrations as long as the displacement amplitude is large enough to be measured, and the frequency is not so high that it cannot be resolved by the timer counting method.
(5) Smaller sensor voltage outputs were seen for the aluminum alloy specimen than for the carbon steel specimen. While tests for both specimens showed similar trends in the linear proportionality constants as a function of frequency, a mapping from sensor voltage output to physical displacement for carbon steel required larger proportionality constants than for aluminum alloy.

According to the test results, the EFB vibration sensor shows promise for measuring dynamic displacements to monitor the health of specimens during resonant fatigue testing. A simple monitoring method using this sensor is to monitor the resonant frequency of one of the low modes. Through calibration tests, sensor voltage outputs could be easily converted to physical displacements. The proposed sensing technique proves to be an efficient method for high-frequency vibration monitoring, especially for resonant fatigue testing, and holds promise for other applications that would benefit from the use of noncontact sensors, such as the monitoring of spindle dynamics, the nondestructive damage evaluation of conductive materials and structural components, and vibration monitoring. Although not addressed in this paper, further characterization of the frequency-dependent nature of the sensor could be used to further develop the EFB vibration sensor to make it suitable for sensing dynamic motion under ambient vibration; this would require the development of a nonlinear, frequency-domain model for calibrating the sensor output.

Acknowledgments

This research was partially supported by the NASA Science Mission Directorate by a grant (200SUB-NAS203128-UOA) from Sunpower Inc., Athens, Ohio under NASA prime contract (NAS3-03128). The authors are particularly grateful to Mr Dave Krause and Dr Kalluri at NASA Glenn Research Center for their support in this research. The first, second and fourth authors are also partially supported by a grant (07 High Tech A01) from the High Tech Urban Development Program funded by the Ministry of Land, Transportation and Maritime Affairs of the Korean government. The authors are grateful for this support, too.

References

[1] Cha Y J, Nam B, Kim J and Kim K H 2010 Evaluation of the planar inductive magnetic field sensors for metallic crack detections *Sensors Actuators* A **162** 13–9
[2] Du L, Zhe J, Carletta J E and Veillette R J 2010 Inductive Coulter counting: detection and differentiation of metal wear particles in lubricant *Smart Mater. Struct.* **19** 1–7
[3] Du L, Zhe J A, Carletta J, Veillette R and Choy F 2010 Real-time monitoring of wear debris in lubrication oil using a microfluidic inductive Coulter counting device *Microfluid. Nanofluid.* **9** 1241–5
[4] Nerino R 1995 Capacitive sensor arrays in dimensional analysis of surfaces *IEEE Trans. Instrum. Meas.* **44** 875–80
[5] Kaito K, Abe M and Fujino Y 2005 Development of non-contact scanning vibration measurement system for real-scale structures *Struct. Infrastruct. Eng.* **1** 189–205
[6] Haddadi H and Belhabib S 2008 Use of rigid-body motion for the investigation and estimation of the measurement errors related to digital image correlation technique *Opt. Lasers Eng.* **46** 185–96
[7] Fericean S and Droxler R 2007 New noncontacting inductive analog proximity and inductive linear displacement sensors for industrial automation *IEEE Sensors J.* **7** 1538–45
[8] Passeraub P A, Besse P A, Bayadroun A, Hediger S, Bernasconi E and Popovic R S 1999 First integrated inductive proximity sensor with on-chip CMOS readout circuit and electrodeposited 1mm flat coil *Sensors Actuators* A **76** 273–8

[9] Passeraub P A, ReyMermet G, Besse P A, Lorenz H and Popovic R S 1997 Inductive proximity sensor with a flat coil and a new differential relaxation oscillator *Sensors Actuators* A **60** 122–6
[10] Kejik P, Kluser C, Bischofberger R and Popovic R S 2004 A low-cost inductive proximity sensor for industrial applications *Sensors Actuators* A **110** 93–7
[11] Mavroyannakis E G 1982 Inductive sensor for the detection of low velocities *J. Phys. E: Sci. Instrum.* **15** 80–2
[12] Yun G J, Nam S B, Carletta J, Binienda W and Kim D H 2009 Vibration based crack detection of conductive beam structures using a non-contact inductive vibration sensor *ANCRiSST: The 5th Int. Workshop on Advanced Smart Materials and Smart Structures Technology (Boston, MA)*
[13] Plonus M A 1978 *Applied Electromagnetics* (New York: McGraw-Hill)
[14] Bray D E and Stanley R K 1997 *Nondestructive Evaluation: A Tool in Design, Manufacturing and Service* (Boca Raton, FL: CRC Press) (London: Taylor and Francis)
[15] Wheeler H A 1928 Simple inductance formulas for radio coils *Proc. IRE* **16** 1398–400